

# Topological effects in the optical phonon dynamics of the three dimensional Dirac semimetal Cd<sub>3</sub>As<sub>2</sub>

A. Sharafiev<sup>1,2</sup>, V. Gnezdilov<sup>1,3</sup>, R. Sankar<sup>4</sup>, F. C. Chou<sup>4</sup>, and P. Lemmens<sup>1,2\*</sup>

<sup>1</sup>*Inst. for Condensed Matter Physics, TU Braunschweig, D-38106 Braunschweig, Germany*

<sup>2</sup>*Laboratory for Emerging Nanometrology, TU Braunschweig, D-38106 Braunschweig,  
Germany*

<sup>3</sup>*B. I. Verkin Inst. for Low Temperature Physics and Engineering, National Academy of  
Sciences of Ukraine, Kharkov 61103, Ukraine*

<sup>4</sup>*Center for Condensed Matter Sciences, National Taiwan University, Taipei 10617, Taiwan*

## Abstract

In the three-dimensional Dirac semimetal Cd<sub>3</sub>As<sub>2</sub> we notice an interplay of electronic and phonon degrees of freedom mediated by topological effects. There exist a pronounced quasielastic scattering and an anomalous anharmonicity of optical phonons. These effects follow a similar temperature dependence with a characteristic temperature  $T^* \sim 100$  K. Furthermore, there exist a resonant enhancement of phonon scattering intensity as function of incident photon energy. This energy of 1.9 eV coincides with interband electronic transitions in Cd<sub>3</sub>As<sub>2</sub><sup>1</sup>. A refined analysis shows that these effects are coupled via interband transitions in the Dirac states in Cd<sub>3</sub>As<sub>2</sub> and a degeneracy of phonon energies with thermally excited electronic states. This degeneracy enhances energy density fluctuations.

**Keywords: Dirac semimetal, phonon dynamics, characteristic temperature**

**\*: Corresponding Author: phone: +49 351-391-5130, email: p.lemmens@tu-bs.de**

## I. INTRODUCTION

Topological semimetals are an interesting and novel state of matter that attract considerable interest in condensed matter physics. There exist relativistic bulk electronic bands with linear dispersion and non-trivial spin texture due to strong spin-orbit coupling, and other prominent features. One of the representatives of this group of materials is  $\text{Cd}_3\text{As}_2$ , which is well known for an anomalously high electron mobility ( $\approx 8.0 \text{ m}^2 \text{ V}^{-1} \text{ s}^{-1}$ ) despite a semimetallic character of conductivity and a complex, defect-ordered structure<sup>2-5</sup>.

Recent studies show two stable Dirac nodes at two special  $k$  points along the G-Z momentum space direction with linear dispersing bands in all three dimensions<sup>6,7,8</sup>. In addition, the Fermi velocity of these 3D Dirac fermions is quite high ( $\approx 2 \cdot 10^6 \text{ m} \cdot \text{s}^{-1}$ )<sup>6</sup> in comparison with the well-studied 2D Dirac systems (e.g. topological insulators). It is about 3 times higher than in the topological surface states of  $\text{Bi}_2\text{Se}_3$ <sup>9</sup> and 1.5 times higher than in graphene<sup>10</sup>.

The existence of 3D Dirac fermions in  $\text{Cd}_3\text{As}_2$  implies that this system is a bulk counterpart of graphene<sup>7</sup>. There are also other 3D topological Dirac semimetals, such as  $A_3\text{Bi}$  ( $A = \text{K}, \text{Rb}, \text{Na}$ )<sup>11</sup> or  $\beta$ -cristobalite  $\text{BiO}_2$ <sup>12</sup>. However, they are all unstable under ambient conditions. In this context,  $\text{Cd}_3\text{As}_2$  stands out with respect to application oriented properties.

Topological Dirac semimetals can be driven into Weyl semimetal or a topological insulator by symmetry breaking or increasing spin-orbit coupling, respectively. Reducing dimensionality a quantum spin Hall insulator is induced<sup>13</sup>. Therefore, the presence or absence of a center of inversion in  $\text{Cd}_3\text{As}_2$  is a crucial parameter which will affect the electronic band structure<sup>14</sup>. The fundamental relationship between the crystalline symmetries and the topological properties of 3D Dirac semimetals is described in Ref. <sup>15</sup> and a generic phase diagram of systems with time-reversal, inversion and rotation symmetries is given. Unfortunately, in literature there are inconsistencies in the interpretation of the symmetry of  $\text{Cd}_3\text{As}_2$  crystal structure. This is based on its complex, defect-ordered structure that could even lead to a local symmetry based on preparation conditions of the samples. Therefore, an independent experimental prove of the symmetry is very important and might help to resolve the disputes concerning the existence of an inversion center and whether  $\text{Cd}_3\text{As}_2$  indeed realized a 3D Dirac system.

Here, we report on results of a Raman scattering study on  $\text{Cd}_3\text{As}_2$  single crystals. This system shows evidence for an intricate interplay of phonons with electronic degrees of freedom leading to a characteristic temperature  $T^* \sim 100 \text{ K}$ .

## II. EXPERIMENTAL DETAILS

Single crystals of  $\text{Cd}_3\text{As}_2$  with dimensions of  $2 \text{ mm}^3$  were grown by self-selecting vapor growth (SSVG) method. Raman scattering measurements were performed in quasi-backscattering geometry from shiny surface of the crystals with a triangular shape which corresponds to the  $\{112\}$  plane<sup>16</sup>. Samples were cleaned with acetone and isopropanol before fixing them on the sample holder using silver glue. Raman spectra were measured in both parallel ( $xx$ ) and crossed ( $yx$ ) polarizations, with incident light polarized perpendicular or parallel to the base of the triangle, respectively.

As excitation sources, solid state ( $\lambda = 532$  and  $488 \text{ nm}$ ) and Ar-Kr-ion ( $\lambda = 488, 514.5, 568, \text{ and } 647 \text{ nm}$ ) lasers were used. The laser power less than  $10 \text{ mW}$  was focused to a  $100\text{-}\mu\text{m}$ -diameter spot on the crystal. Note that in the present experiments we used a power of the exciting radiation that is at least 20 times smaller than in previous Raman experiments on  $\text{Cd}_3\text{As}_2$ <sup>17,18</sup>.

The spectra were collected via a triple spectrometer (Dilor-XY-500) by a liquid nitrogen cooled CCD (Horiba Jobin Yvon, Spectrum One CCD-3000V). Temperature dependencies from  $9 \text{ K}$  to  $300 \text{ K}$  of the Raman spectra were measured in a variable temperature closed cycle cryostat (Oxford/Cryomech Optistat).

## III. RESULTS

*Crystal structure and phonon spectra.* The crystal structure of  $\text{Cd}_3\text{As}_2$  is complicated and can be related to tetragonally distorted antiferroite structure with  $1/4$  Cd site vacancies. At high temperatures ( $T > 873 \text{ K}$ ), the distribution of these vacancies is random and leads to the ideal antiferroite space group  $Fm\bar{3}m$ . In the temperature region of  $873 \text{ K} > T > 648 \text{ K}$ , Cd ions are ordered leading to  $P4_2/nmc$ <sup>14</sup>. At lower temperatures, the crystal structure of  $\text{Cd}_3\text{As}_2$  was initially determined as non-centrosymmetric ( $I4_1cd$ )<sup>19</sup> and finally proposed to be centrosymmetric ( $I4_1acd$ )<sup>14</sup>. Resolving the ambiguity between centrosymmetric and noncentrosymmetric crystal structures can be difficult in some cases and this is a well-known problem in crystallography<sup>20,21</sup>. Raman scattering reveals itself as an effective tool to refine the crystal structure based on the number of observed phonon modes.

The factor group analysis yields 145 Raman-active phonon modes ( $\Gamma_{\text{Raman}} = 26A_1 + 27B_1 + 27B_2 + 65E$ ) for noncentrosymmetric  $I4_1cd$  (No 110,  $Z = 16$ ) and 74 modes for centrosymmetric  $I4_1acd$  (No 142,  $Z=32$ ). The corresponding Raman tensors are, respectively:

$$A_1 = \begin{pmatrix} a & 0 & 0 \\ 0 & a & 0 \\ 0 & 0 & b \end{pmatrix}, \quad B_1 = \begin{pmatrix} c & 0 & 0 \\ 0 & -c & 0 \\ 0 & 0 & 0 \end{pmatrix}, \quad B_2 = \begin{pmatrix} 0 & d & 0 \\ d & 0 & 0 \\ 0 & 0 & 0 \end{pmatrix},$$

$$E(x) = \begin{pmatrix} 0 & 0 & e \\ 0 & 0 & 0 \\ e & 0 & 0 \end{pmatrix}, \quad E(y) = \begin{pmatrix} 0 & 0 & 0 \\ 0 & 0 & e \\ 0 & e & 0 \end{pmatrix};$$

$$A_{1g} = \begin{pmatrix} a & 0 & 0 \\ 0 & a & 0 \\ 0 & 0 & b \end{pmatrix}, \quad B_{1g} = \begin{pmatrix} c & 0 & 0 \\ 0 & -c & 0 \\ 0 & 0 & 0 \end{pmatrix}, \quad B_{2g} = \begin{pmatrix} 0 & d & 0 \\ d & 0 & 0 \\ 0 & 0 & 0 \end{pmatrix},$$

$$E_g = \begin{pmatrix} 0 & 0 & -e \\ 0 & 0 & e \\ -e & e & 0 \end{pmatrix}.$$

Since Raman measurements were done on a natural cleavage  $\{112\}$  plane, all possible Raman-active phonon modes are expected in the spectra for every polarization configuration. In previous Raman experiments in  $\text{Cd}_3\text{As}_2$  only nine phonon modes have been observed<sup>17,18</sup>. Our data show a much larger number of phonons in  $\text{Cd}_3\text{As}_2$  that can be divided into two frequency regimes, below  $80 \text{ cm}^{-1}$  and  $150 - 250 \text{ cm}^{-1}$ . We attribute them to collective vibrations of mainly Cd coordinations and As phonons, respectively. Using a  $\lambda = 532 \text{ nm}$  laser excitation line with a power of  $20 \text{ mW}$  there are 13 modes at room temperature and 27 lines at low temperatures, see Fig. 1. The spectra in  $(xx)$  polarization are superposed by a pronounced and extended quasielastic (QE) signal observed at high temperatures. This scattering will be discussed further below.

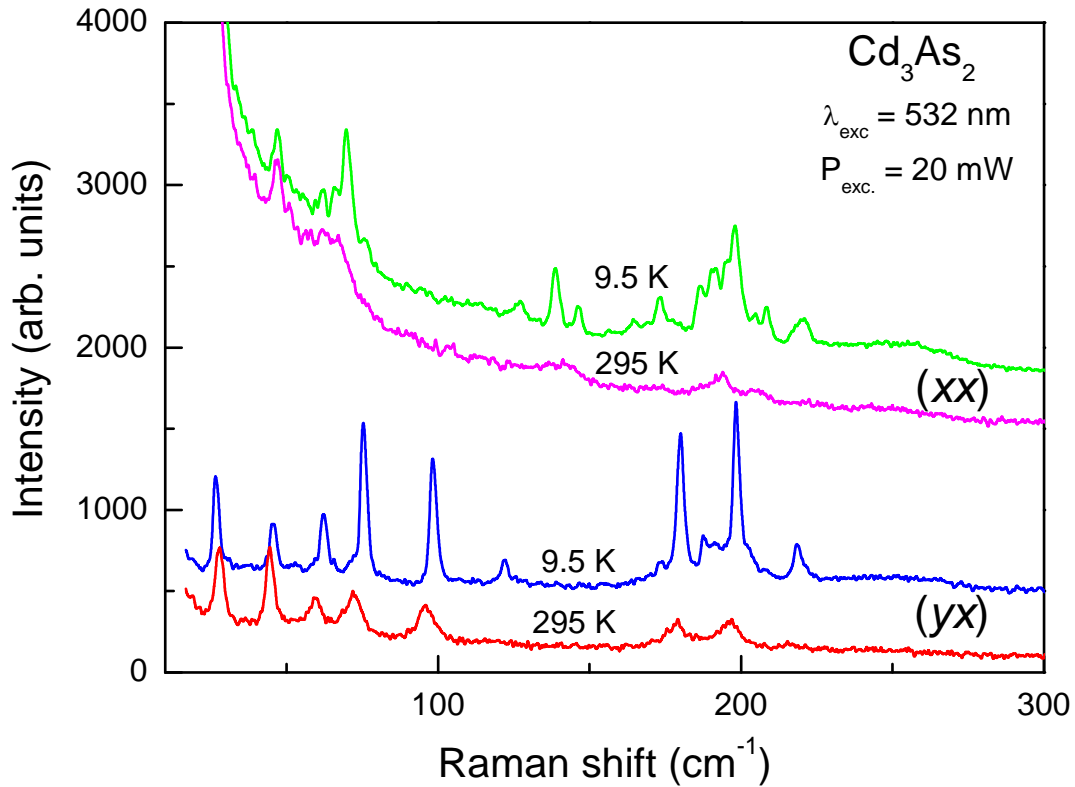


Figure 1. Raman spectra of Cd<sub>3</sub>As<sub>2</sub> taken with  $\lambda = 532 \text{ nm}$  excitation line, (xx) and (yx) polarizations, at T= 9.5 K and room temperature, respectively.

There exist a pronounced dependence of the Raman scattering intensity on the energy of the incident radiation. This resonance effect depends on the investigated signal, indicating that distinctively different electronic states are involved in the Raman intermediate states. We performed a detailed resonance study of the 150-250 cm<sup>-1</sup> integrated intensity and of the QE scattering, as shown in Fig. 2 and its inset. The largest enhancement of phonons exist at the excitation of  $\lambda = 647 \text{ nm}$  (1.9 eV). This wavelength coincides with an intrinsic electronic transition of Cd<sub>3</sub>As<sub>2</sub> as observed in reflectivity spectra of Cd<sub>3</sub>As<sub>2</sub><sup>1</sup>. The QE scattering shows its largest intensity at the smallest wavelength of  $\lambda = 488 \text{ nm}$  (2.54 eV).

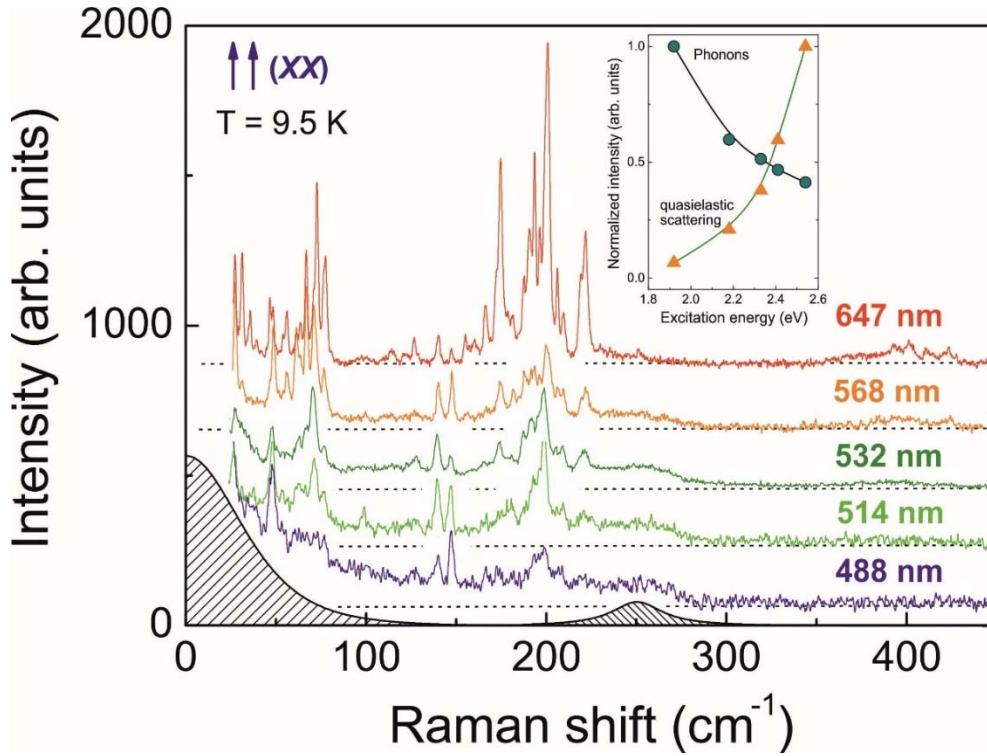


Figure 2. Raman spectra of Cd<sub>3</sub>As<sub>2</sub> with different incident laser excitations, (xx) polarization, and  $T = 9.5$  K. The dashed lines correspond to the background. The dashed areas represent a fitting of the QE scattering and a plasmon maximum at  $250\text{ cm}^{-1}$  to the 488-nm data, as described in the text. The inset shows the normalized intensity of the QE scattering and the phonons as function of excitation wavelength. The phonon intensity is integrated in the regime  $150\text{-}250\text{ cm}^{-1}$  and corrected for a background.

In the following we will focus on the  $\lambda = 647$  nm excitation as the phonon lines are well distinguished and have largest intensities. Selected temperature dependent Raman spectra of Cd<sub>3</sub>As<sub>2</sub> are shown in Fig. 3. A detailed list of the phonon modes is given in Table I. The spectra are fitted by Lorentzian profiles with a typical result shown in Fig. 4. The number of 44 observed phonon modes allows us to support the centrosymmetric ( $I4_1acd$ ) structure since the non-centrosymmetric ( $I4_1cd$ ) structure should show a significantly larger number of phonon modes in Raman scattering. There also exist pronounced phonon anomalies as function of temperature. For the low energy modes this can be easily quantified by fitting, see Fig. 5. For the higher frequency phonons also anomalous properties are noted, especially a strong broadening of linewidth. However, due to the close proximity of the modes an individual fitting is not viable. Two phonon scattering is observed at approximately  $400\text{ cm}^{-1}$ .

Table I. List of the 44 phonon modes of Cd<sub>3</sub>As<sub>2</sub> determined at T=9.5K and  $\lambda = 647$  nm excitation. Highest intensity is denoted by “+++”, while “-” denotes zero intensity.

$\omega$ (cm <sup>-1</sup> )	XX	XY	Assignment	$\omega$ (cm <sup>-1</sup> )	XX	XY	Assignment
27.4	+++	+	B <sub>1g</sub>	155	++	+	B <sub>2g</sub>
31.2	+++	-	A <sub>1g</sub>	157.2	+	+	B <sub>2g</sub>
35.6	+	-	A <sub>1g</sub>	160.1	+	-	A <sub>1g</sub>
39.3	++	+	B <sub>2g</sub>	166.4	+++	+	B <sub>1g</sub>
46.7	+	++	E <sub>g</sub>	172.2	+	-	A <sub>1g</sub>
48.3	+	+	B <sub>2g</sub>	174.7	+++	+	B <sub>1g</sub>
53.9	++	+	B <sub>2g</sub>	177.8	+	-	A <sub>1g</sub>
56	+++	+	B <sub>1g</sub>	181.4	+	++	E <sub>g</sub>
59.9	-	+	E <sub>g</sub>	187.5	+++	+	B <sub>1g</sub>
61.5	+	-	A <sub>1g</sub>	190.4	+++	+	B <sub>1g</sub>
63.6	+	++	E <sub>g</sub>	191.6	++	+	B <sub>2g</sub>
66.8	+++	+	B <sub>1g</sub>	193.6	+++	+	B <sub>1g</sub>
70.8	+	-	A <sub>1g</sub>	196.4	+++	+	B <sub>1g</sub>
72.8	+++	+	B <sub>1g</sub>	199.2	+++	+	B <sub>1g</sub>
76.3	+	++	E <sub>g</sub>	201	+++	+	B <sub>1g</sub>
77.6	+	++	E <sub>g</sub>	204.1	-	+	E <sub>g</sub>
98.7	+	++	E <sub>g</sub>	206.3	+++	+	B <sub>1g</sub>
114.2	+	-	A <sub>1g</sub>	209.6	+	-	A <sub>1g</sub>
121.7	+	-	A <sub>1g</sub>	218.9	+	-	A <sub>1g</sub>
126.8	+	+	B <sub>2g</sub>	220.2	-	+	E <sub>g</sub>
140	+	-	A <sub>1g</sub>	220.8	-	+	E <sub>g</sub>
147.4	+	-	A <sub>1g</sub>	221.8	+	-	A <sub>1g</sub>

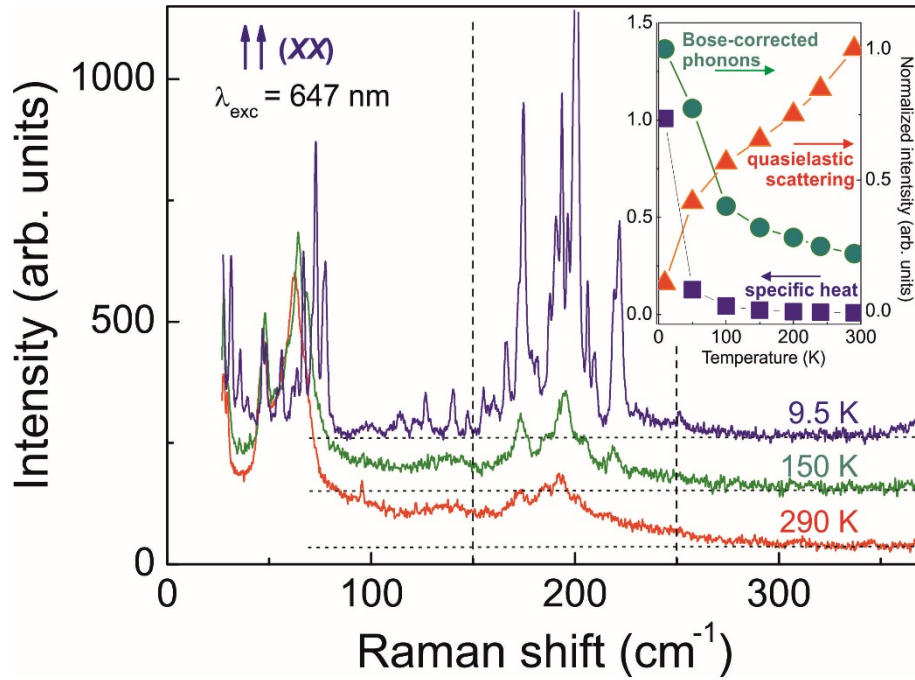


Figure 3. Raman spectra of Cd<sub>3</sub>As<sub>2</sub> at three selected temperatures measured in (xx) polarization and  $\lambda = 647 \text{ nm}$ . The data is shifted and dashed lines mark the background. The inset shows the normalized intensity of the QE scattering, the specific heat  $C_p^{\text{fluct}}$  based on QE scattering by a scaling with  $T^2$ , and the Bose-corrected phonon scattering as function of temperature, respectively. The latter is determined by an integration within the frequency regime 150-250 cm<sup>-1</sup>.

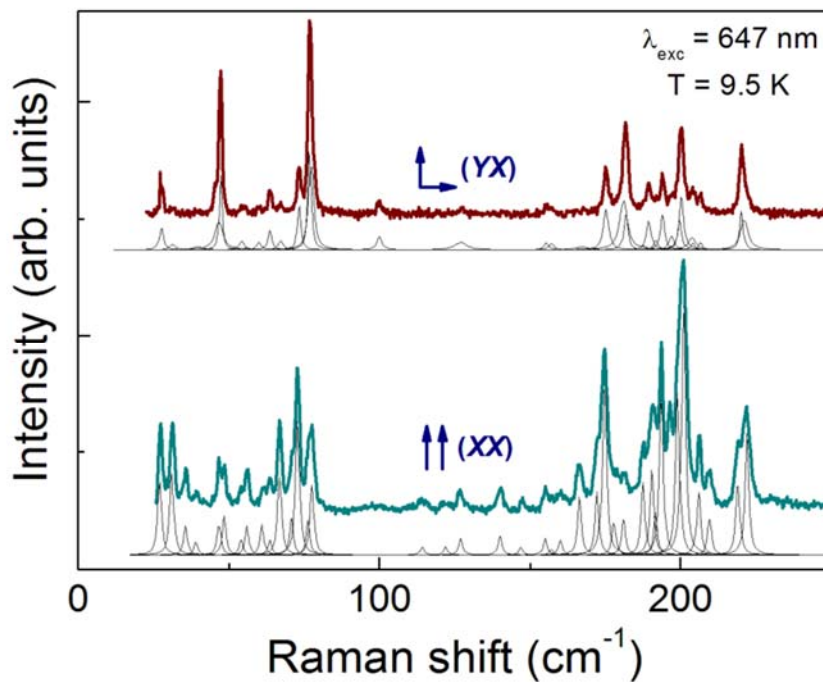


Figure 4. Low temperature Raman spectra of Cd<sub>3</sub>As<sub>2</sub> at  $T = 9.5 \text{ K}$  in (xx) and (yx) polarizations. Black lines show fits to the phonon modes from Table 1 using Lorentzians.



In Fig. 5 the temperature dependence of the phonon frequencies  $\omega(T)$  and linewidths  $\Gamma(T)$  (FWHM) of selected phonon modes (46.5, 48.5, 67 and 73  $\text{cm}^{-1}$ ) are given. There exist pronounced changes in slope that are not in accordance with the expected anharmonicity based on multi-phonon scattering processes. To highlight these effects the data are plotted together with full lines that correspond to effects due to cubic anharmonic interactions<sup>22-24</sup>. Within this approximation occupation factors of frequency averaged, decaying phonons  $\omega_{av3}$  and  $\omega_{av4}$  are weighted by scaling factors  $b_j$  and  $c_j$  are used to describe three- and four-particle processes:

$$\omega_j(T) = \omega_{0j} - \frac{b_j}{\exp(\hbar\omega_{av3}/k_B T) - 1} - \frac{c_j}{\exp(\hbar\omega_{av4}/k_B T) - 1} - \frac{c_j}{[\exp(\hbar\omega_{av4}/k_B T) - 1]^2},$$

here,  $\omega_{0j}$  is the eigenfrequency of the phonon at  $T = 0$  K. In simplest approximation the frequency of the decaying phonons are  $\omega_{av3} \approx \omega_{0j}/2$  and  $\omega_{av4} \approx \omega_{0j}/3$ .

The phonon linewidth is described in a related way,

$$\Gamma_j(T) = \Gamma_{0j} + \frac{d_j}{\exp(\hbar\omega_{0j}/2k_B T) - 1} + \frac{f_j}{\exp(\hbar\omega_{0j}/3k_B T) - 1} + \frac{f_j}{[\exp(\hbar\omega_{0j}/3k_B T) - 1]^2},$$

where  $\Gamma_0$ ,  $\omega_0$ ,  $d_j$ , and  $f_j$  are the width, eigenfrequency at  $T = 0$  K, and mode dependent parameters for three- and four-particle decay and coalescence processes, respectively.

The deviations from the approximated anharmonic effects and the experimental data are substantial. This should be regarded as strong evidence for additional relaxation mechanism that the optical phonons are involved in. Based on the observed smooth and continuous shown in the insets of Fig. 5a and b with a broad maximum and a sharper decrease for temperatures  $T < 100\text{K}$  it is obvious that temperature itself is only a weak controlling parameter. Therefore, we rule out a purely structural origin of this deviation. In contrast we consider other degrees of freedom, i.e. a coupling of the phonons to electronic degrees of freedom.

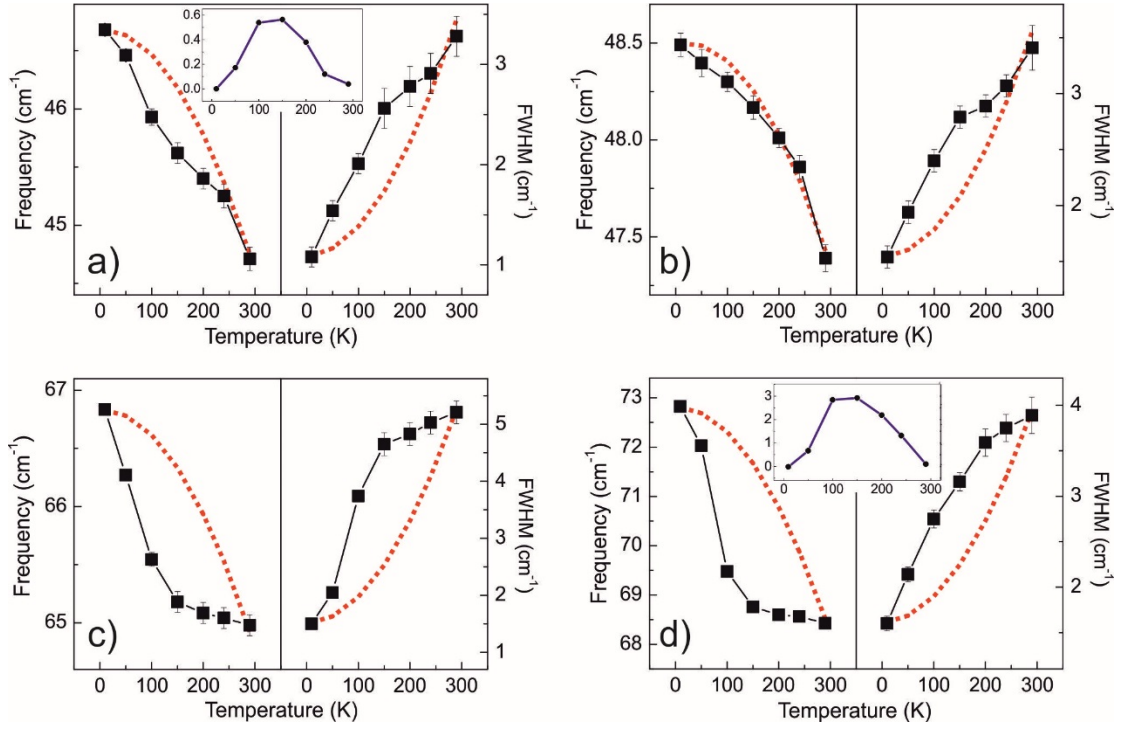


Figure 5. Temperature dependence of the phonon frequencies and linewidths for the modes at (a)  $46.5 \text{ cm}^{-1}$ , (b)  $48.5 \text{ cm}^{-1}$ , (c)  $67 \text{ cm}^{-1}$ , and (d)  $73 \text{ cm}^{-1}$ . The dashed red lines approximate anharmonic variation of phonons with temperature. The insets in a) and d) show the respective deviation of measured and approximated phonon frequency with temperature.

*Quasielastic scattering.* In the following we will focus on QE scattering. Such contributions are characterized by small characteristic energy shifts, i.e. shifts below the phonon energy range. Their detection requires a careful alignment of the pre-monochromator of the spectrometer that defines the bandpass of the resolved spectrum. Thereby it is ensured that elastically scattered light from surfaces of the optics and the crystal do not overcome the limited stray light rejection of the final stage of the spectrometer and are resolved as QE.

The data presented in Fig. 1 to Fig. 3 may be summarized as follows: QE scattering in  $\text{Cd}_3\text{As}_2$  has a linewidth of approximately  $100 \text{ cm}^{-1}$  and a dominant contribution in (xx) polarization. The integrated spectral weight is largest at high temperatures and shows a strong suppression for temperatures  $T < 100 \text{ K}$ , see inset of Fig. 3. Such a temperature dependence is a strong argument towards an intrinsic origin as extrinsic effects are expected to be independent of temperature. The derived fluctuation induced specific heat  $C_p^{\text{fluct}}(T) \propto I_{\text{quasiel}} / T^2$  shows a temperature dependence similar to the phonon intensity<sup>25</sup>. This scaling is based on energy density fluctuations as discussed further below. Also the phonon parameters show an anomalous temperature dependence for  $T < 100\text{K}$ .

As mentioned above, QE scattering shows a resonant enhancement in the high energy limit,  $\omega_i > 2.9 \text{ eV}$ , see inset Fig. 2. This property differs from phonon scattering which is

resonant for  $\omega_i \sim 1.9$  eV<sup>26</sup>. This implies that phonon scattering and QE scattering involve different intermediate states in the Raman scattering process. Unfortunately, the available data does not allow determining a clear functional dependence<sup>27</sup> of the resonance. The QE intensity drops too fast at smaller excitation energies.

To analyze the lineshape of the QE scattering we choose the  $\lambda=488$  nm-data with the highest related scattering intensity, We fitted the QE signal with the following equation:

$$I(\omega) = I_0 / (((2^{\sqrt{N}} - 1)(\omega - \omega_0) / \gamma)^2 + 1)^N,$$

where  $I_0$  is intensity at the frequency position,  $\omega_0$  is the line maximum. With the parameter  $N = 1$  a pure Lorentzian line shape is resolved, while large  $N$  ( $\sim 200$ ) leads to a Gaussian line shape. The fit to the experimental data given by the dashed area in Fig. 2 (shifted in intensity) corresponds to  $N \approx 2.7$ . Therefore we conclude a Lorentzian line shape of this process.

#### IV. DISCUSSION

QE scattering in semimetals without a structural instability and spin degrees of freedom should be attributed to electronic excitations. The latter can be related to Lorentzian energy density fluctuations or charge density fluctuations, i.e. Gaussian fluctuations of the electron distribution function<sup>28</sup>. A common feature of these processes is that the energy  $\hbar\omega$  and the transferred momentum  $\hbar q$  are small. In Cd<sub>3</sub>As<sub>2</sub> we assume energy density fluctuations to be the origin of the QE scattering based on the observed symmetry and Lorentzian line shape.

There is a similarity of our observations in Cd<sub>3</sub>As<sub>2</sub> to low dimensional spin systems<sup>29</sup>. Here, pronounced QE scattering exist and is related to the suppression of long range magnetic. Detailed studies also show phonon anomalies with an unspecific temperature dependence. Generally speaking, such anomalies are related to the tendency of the coupled spin and phonon systems to reduce degeneracies of the spin system. Here we refer to the spin system (VO)<sub>2</sub>P<sub>2</sub>O<sub>7</sub><sup>30</sup> and the spin/charge system  $\alpha'$ -NaV<sub>2</sub>O<sub>5</sub><sup>31</sup>, respectively, as examples. Within the approach of energy density fluctuations the QE scattering intensity is based on a coupling of the spins to the phonon “bath”. This coupling increases its linewidth to the spin-lattice relaxation rate. Its intensity is given by  $I_{\text{quasiel.}} \propto C_p^{\text{fluct}} \cdot T^2$ <sup>25</sup>. This scaling works rather effectively allowing estimates of the spin entropy as function of temperature<sup>32</sup>.

From the inset of Fig. 3 we notice that  $C_p^{\text{fluct}}$  derived for Cd<sub>3</sub>As<sub>2</sub> shows a rapid increase for  $T < 100$ K. Its temperature dependence is similar to that of the Bose corrected integrated phonon scattering intensity. The latter quantity is related to the electronic polarizability of the system with respect to atomic displacements. Similarly, in this temperature range deviations from conventional phonon anharmonicity evolve, see Fig. 5 and its insets.

At this point it might be useful to consider again the specific properties of the phonon system of  $\text{Cd}_3\text{As}_2$ . Based on its complex, defect ordered structure<sup>14</sup> we expect that the low frequency phonon modes couple to the Dirac states close to the Fermi Energy. This is due to the role of Cd vacancies leading to channels which lift or preserve the inversion symmetry needed for the Dirac semimetal. On the other side, such a lattice tends to a dense spectrum of low energy phonon modes which are partially localized due to some randomness of the vacancy sites.

Indeed we observe a huge number of modes distributed in two bands at  $150 - 250 \text{ cm}^{-1}$  ( $\equiv 220 - 360 \text{ K}$ ) as well as below approximately  $80 \text{ cm}^{-1}$  ( $\equiv 110 \text{ K}$ ), Figs. 2 and 3. These two frequency bands are assigned to individual Cd and As vibrations and to groups of heavy atoms on the Cd cubes that perform rotations and distortions, respectively. Considering a thermal population of these bands according to the Bose factor, a temperature variation in the range of the quasi-gap of phonons will lead to strong variations of the occupied states. Thereby all physical properties related to the phonon density of states will react. These are transport properties, like resistivity, but also the phonon linewidth and others related to anharmonicity.

On the other side there exist a back-action of the phonon self-energy (frequency and lifetime) with topological properties of the electronic states. This means that the role of the phonon system goes beyond that of the above mentioned phonon bath<sup>33</sup>. This is based on the modification of electron-phonon matrix elements with a topological band inversion<sup>34</sup>. With an existing electronic band gap intraband (particle-hole pair) scattering leads to an enhanced phonon linewidth and gradual variations of the phonon frequency for small momenta. In the case of small or negligible gaps interband processes are important for phonons with larger momenta. For topological insulators the magnitude of phonon effects is of the order of a few  $\text{cm}^{-1}$ <sup>33</sup> in good agreement with several experimental studies<sup>35-37</sup>. In contrast, experimental studies of related phonon effects in Dirac semimetals remain rare. This may be due to the limitation of effects to phonons with larger momenta. However, the anharmonicity of optical phonons with  $k \propto 0$  involves a coupling to phonons at the zone boundary. Therefore interband scattering processes in the Dirac states can contribute to some extent to the self-energy of optical phonons.

Interestingly, the largest anharmonic anomalies as well as intensity gains are observed for phonons which are very close to the lower and upper threshold of the quasi-gap. Taking these data together with the evolution of  $C_p^{\text{fluct}}$  motivates the assumption that in  $\text{Cd}_3\text{As}_2$  the energy of relevant phonons that couple to Dirac states and that of the characteristic temperatures, i.e.  $T^* \sim 100 \text{ K}$  match. We propose that this degeneracy allows enhanced fluctuations.

In some transport studies similar characteristic temperature scales have been demonstrated. In  $\text{Cd}_3\text{As}_2$  microbelts with ultrahigh mobility the derived carrier density shows

a minimum at 150K and a following increase towards low temperatures<sup>38</sup>. In another experiment an anomalously large Nernst effect is only observed below 50 K and attributed to the temperature evolution of the transport relaxation rate<sup>39</sup>. In Hall effect measurements on nanoplates the largest changes of the transverse conductivity with field are observed between 80 and 100 K together with a transition in the type of conduction<sup>40</sup>. In a critical discussion of these effects, however, finite doping, i.e. the shift of the  $E_F$  from the Dirac cone should be taken into account. In a recent investigation of optical conductivity it has been shown that such a charge carrier crossover at  $T^* = 100$  K is compatible with a Fermi energy of  $E_F \approx 25$  meV<sup>41</sup>. This is based on thermally excited carriers and a resulting temperature dependent chemical potential.

Finally we address evidence for scattering processes on the Dirac states using the Raman process, as single particle or collective excitations (plasmon-like). Such processes could evade screening by an electronic mass anisotropy or strong defect scattering. Evidences for electronic Raman scattering in Dirac electron systems have previously been found in carbon nanotubes<sup>42</sup> and Rashba semimetals<sup>43</sup>. The corresponding effects consist of broad Gaussian maxima and range in energy from  $\Delta\omega = 40$  cm<sup>-1</sup> to 500 cm<sup>-1</sup>. In Cd<sub>3</sub>As<sub>2</sub> we observe one Gaussian maximum at  $\omega_{\text{plas}} = 250$  cm<sup>-1</sup> with a width (FWHM) of  $\Gamma = 30$  cm<sup>-1</sup> that fits both in energy and linewidth to this scenario. For optical conductivity it is expected that the Dirac electron system contributes in a very different way. Here a linear additional component is expected with an onset for frequencies  $\omega > \omega_{\text{Pauli}} = 2E_F$ , which is the Pauli-blockade energy. In very thin crystals of the Dirac semimetal ZrTe<sub>5</sub> such an effect has been observed at 120 cm<sup>-1</sup><sup>44</sup>, while in Cd<sub>3</sub>As<sub>2</sub> it has not been resolved up to now<sup>45</sup>.

#### IV. CONCLUSIONS

In our Raman scattering study of the three-dimensional Dirac semimetal Cd<sub>3</sub>As<sub>2</sub> for the first time a number of phonon lines compatible with a centrosymmetric structure (*I4<sub>1</sub>acd*) has been observed. A resonant enhancement of phonon scattering is observed with an excitation of 1.9 eV. This energy corresponds to the energy of the interband electronic transition observed earlier in reflectivity measurements. There exist evidence for a characteristic temperature scale in the phonon frequency, linewidth and intensity, as well as in a quasielastic scattering component. We describe the phonon effects as due to an anharmonic phonon scattering processes that couples to interband excitations in the Dirac states. The strong quasielastic scattering is attributed to energy density fluctuations of the coupled electron-phonon system. The observed characteristic temperature scale  $T^* \sim 100$  K is most probably related to a matching of characteristic energies of important phonons with temperature scales induced by thermally activated carriers in the Dirac electron states.

## ACKNOWLEDGEMENTS

We thank David Schmeltzer and Ion Garate for important discussions. We would like to acknowledge the support of the International Graduate School of Metrology (B-IGSM) and the Graduate School Contacts in Nanosystems. Financial support by GIF and DFG-RTG 1952 Nanomet, and DFG-LE967/16-1 is appreciated.

---

1. Karnicka-Moscicka, K., Kisiel, A. & Zdanowicz, L. Fundamental reflectivity spectra of monocrystalline and polycrystalline bulk Cd<sub>3</sub>As<sub>2</sub>. *Solid State Commun.* **44**, 373–377 (1982).
2. Rosenberg, A. J. & Harman, T. C. Cd<sub>3</sub>As<sub>2</sub> - A Noncubic Semiconductor with Unusually High Electron Mobility. *J. Appl. Phys.* **30**, 1621–1622 (1959).
3. Lin-Chung, P. J. Energy-Band Structures of Cd<sub>3</sub>As<sub>2</sub> and Zn<sub>3</sub>As<sub>2</sub>. *Phys. Rev.* **188**, 1272–1280 (1969).
4. Zdanowicz, W. & Zdanowicz, L. Semiconducting Compounds of the AII BV Group. *Annu. Rev. Mater. Sci.* **5**, 301–328 (1975).
5. Jay-Gerin, J.-P., Aubin, M. J. & Caron, L. G. The electron mobility and the static dielectric constant of Cd<sub>3</sub>As<sub>2</sub> at 4.2 K. *Solid State Commun.* **21**, 771–774 (1977).
6. Neupane, M. *et al.* Observation of a three-dimensional topological Dirac semimetal phase in high-mobility Cd<sub>3</sub>As<sub>2</sub>. *Nat. Commun.* **5**, 3786 (2014).
7. Liu, Z. K. *et al.* A stable three-dimensional topological Dirac semimetal Cd<sub>3</sub>As<sub>2</sub>. *Nat. Mater.* **13**, 677–81 (2014).
8. Borisenko, S. *et al.* Experimental Realization of a Three-Dimensional Dirac Semimetal. *Phys. Rev. Lett.* **113**, 27603 (2014).
9. Xia, Y. *et al.* Observation of a large-gap topological-insulator class with a single Dirac cone on the surface. *Nat. Phys.* **5**, 398–402 (2009).
10. Bostwick, A., Ohta, T., Seyller, T., Horn, K. & Rotenberg, E. Quasiparticle dynamics in graphene. *Nat. Phys.* **3**, 36–40 (2006).
11. Liu, Z. K. *et al.* Discovery of a three-dimensional topological Dirac semimetal, Na<sub>3</sub>Bi. *Science* **343**, 864–7 (2014).
12. Young, S. M. *et al.* Dirac semimetal in three dimensions. *Phys. Rev. Lett.* **108**, 140405 (2012).
13. Wan, X., Turner, A. M., Vishwanath, A. & Savrasov, S. Y. Topological semimetal and Fermi-arc surface states in the electronic structure of pyrochlore iridates. *Phys. Rev. B* **83**, 205101 (2011).
14. Ali, M. N. *et al.* The crystal and electronic structures of Cd(3)As(2), the three-

- dimensional electronic analogue of graphene. *Inorg. Chem.* **53**, 4062–7 (2014).
15. Yang, B.-J. & Nagaosa, N. Classification of stable three-dimensional Dirac semimetals with nontrivial topology. *Nat. Commun.* **5**, 4898 (2014).
  16. Sankar, R. *et al.* Large single crystal growth, transport property, and spectroscopic characterizations of three-dimensional Dirac semimetal Cd<sub>3</sub>As<sub>2</sub>. *Sci. Rep.* **5**, 12966 (2015).
  17. Jandl, S., Desgreniers, S., Carlone, C. & Aubin, M. J. The Raman Spectrum of Cd<sub>3</sub>As<sub>2</sub>. *J. Raman Spectrosc.* **15**, 137–138 (1984).
  18. Weszka, J., Renucci, M. & Zwick, A. Some aspects of raman scattering in Cd<sub>3</sub>As<sub>2</sub> single crystals. *Phys. status solidi* **133**, 57–64 (1986).
  19. Steigmann, G. A., Goodyear, J. & IUCr. The crystal structure of Cd<sub>3</sub>As<sub>2</sub>. *Acta Crystallogr. Sect. B Struct. Crystallogr. Cryst. Chem.* **24**, 1062–1067 (1968).
  20. Ermer, O. & Dunitz, J. D. Least-squares refinement of centrosymmetric trial structures in non-centrosymmetric space groups. A warning. *Acta Crystallogr. Sect. A* **26**, 163–163 (1970).
  21. Marsh, R. E. Centrosymmetric or noncentrosymmetric? *Acta Crystallogr. Sect. B Struct. Sci.* **42**, 193–198 (1986).
  22. Wakamura, K. & Arai, T. Effect of magnetic ordering on phonon parameters for infrared active modes in ferromagnetic spinel CdCr<sub>2</sub>S<sub>4</sub>. *J. Appl. Phys.* **63**, 5824 (1988).
  23. Klemens, P. G. Anharmonic Decay of Optical Phonons. *Phys. Rev.* **148**, 845–848 (1966).
  24. Balkanski, M., Wallis, R. F. & Haro, E. Anharmonic effects in light scattering due to optical phonons in silicon. *Phys. Rev. B* **28**, 1928–1934 (1983).
  25. Reiter, G. F. Light scattering from energy fluctuations in magnetic insulators. *Phys. Rev. B* **13**, 169–173 (1976).
  26. Gillet, Y., Giantomassi, M. & Gonze, X. First-principles study of excitonic effects in Raman intensities. *Phys. Rev. B* **88**, 94305 (2013).
  27. Cardona, M. & Klein, M. in 147–204 (Springer Berlin Heidelberg, 1983).  
doi:10.1007/3-540-11913-2\_4
  28. Bairamov, B. H., Ipatova, I. P. & Voitenko, V. A. Raman scattering from current carriers in solids. *Physics Reports* **229**, 221–290 (1993).
  29. Lemmens, P., Güntherodt, G. & Gros, C. Magnetic light scattering in low-dimensional quantum spin systems. *Phys. Rep.* **375**, 1–103 (2003).
  30. Grove, M. *et al.* Magnetoelastic coupling and spin excitations in the spin-gap system (VO)<sub>2</sub>P<sub>2</sub>O<sub>7</sub>: A Raman scattering study. *Phys. Rev. B* **61**, 6126–6132 (2000).
  31. Sherman, E. Y., Fischer, M., Lemmens, P., Loosdrecht, P. H. M. van & Güntherodt, G.

- Electron-phonon and spin-phonon coupling in NaV<sub>2</sub>O<sub>5</sub> : Charge fluctuations effects. *Europhys. Lett.* **48**, 648–654 (1999).
32. Lemmens, P. *et al.* Collective Singlet Excitations and Evolution of Raman Spectral Weights in the 2D Spin Dimer Compound SrCu<sub>2</sub>(BO<sub>3</sub>)<sub>2</sub>. *Phys. Rev. Lett.* **85**, 2605–2608 (2000).
  33. Garate, I. Phonon-Induced Topological Transitions and Crossovers in Dirac Materials. *Phys. Rev. Lett.* **110**, 46402 (2013).
  34. Saha, K., Légaré, K. & Garate, I. Detecting Band Inversions by Measuring the Environment: Fingerprints of Electronic Band Topology in Bulk Phonon Linewidths. *Phys. Rev. Lett.* **115**, 176405 (2015).
  35. Kondo, T. *et al.* Anomalous Dressing of Dirac Fermions in the Topological Surface State of Bi<sub>2</sub>Se<sub>3</sub>, Bi<sub>2</sub>Te<sub>3</sub>, and Cu-Doped Bi<sub>2</sub>Se<sub>3</sub>. *Phys. Rev. Lett.* **110**, 217601 (2013).
  36. Zhu, X. *et al.* Electron-Phonon Coupling on the Surface of the Topological Insulator Bi<sub>2</sub>Se<sub>3</sub> Determined from Surface-Phonon Dispersion Measurements. *Phys. Rev. Lett.* **108**, 185501 (2012).
  37. Howard, C. & El-Batanouny, M. Connecting electron and phonon spectroscopy data to consistently determine quasiparticle-phonon coupling on the surface of topological insulators. *Phys. Rev. B* **89**, 75425 (2014).
  38. Chen, Z.-G. *et al.* Scalable Growth of High Mobility Dirac Semimetal Cd<sub>3</sub>As<sub>2</sub> Microbelts. *Nano Lett.* **15**, 5830–5834 (2015).
  39. Liang, T. *et al.* Anomalous Nernst Effect in Dirac Semimetal Cd<sub>3</sub>As<sub>2</sub>. (2016). at <http://arxiv.org/abs/1610.02459>
  40. Li, C.-Z. *et al.* Two-Carrier Transport Induced Hall Anomaly and Large Tunable Magnetoresistance in Dirac Semimetal Cd<sub>3</sub>As<sub>2</sub> Nanoplates. *ACS Nano* **10**, 6020–6028 (2016).
  41. Jenkins, G. S. *et al.* Three-dimensional Dirac cone carrier dynamics in Na<sub>3</sub>Bi and Cd<sub>3</sub>As<sub>2</sub>. *Phys. Rev. B* **94**, 85121 (2016).
  42. Farhat, H. *et al.* Observation of Electronic Raman Scattering in Metallic Carbon Nanotubes. *Phys. Rev. Lett.* **107**, 157401 (2011).
  43. Gnezdilov, V. *et al.* Enhanced quasiparticle dynamics of quantum well states: The giant Rashba system BiTeI and topological insulators. *Phys. Rev. B* **89**, 195117 (2014).
  44. Chen, R. Y. *et al.* Optical spectroscopy study of the three-dimensional Dirac semimetal ZrTe<sub>5</sub>. *Phys. Rev. B* **92**, 75107 (2015).
  45. Neubauer, D. *et al.* Interband optical conductivity of the [001]-oriented Dirac semimetal Cd<sub>3</sub>As<sub>2</sub>. *Phys. Rev. B* **93**, 121202 (2016).